Accepted Manuscript

Cooperative path planning with applications to target tracking and obstacle avoidance for multi-UAVs

Peng Yao, Honglun Wang, Zikang Su

PII: S1270-9638(16)30130-4
DOI: http://dx.doi.org/10.1016/j.ast.2016.04.002
Reference: AESCTE 3630

To appear in: *Aerospace Science and Technology*

Received date: 2 November 2015
Revised date: 21 January 2016
Accepted date: 2 April 2016

Please cite this article in press as: P. Yao et al., Cooperative path planning with applications to target tracking and obstacle avoidance for multi-UAVs, *Aerosp. Sci. Technol.* (2016), http://dx.doi.org/10.1016/j.ast.2016.04.002

Cooperative path planning with applications to target tracking and obstacle avoidance for multi-UAVs

Peng Yao[1,2], Honglun Wang[1,2*], Zikang Su[1,2]

(1.School of Automation Science and Electrical Engineering, Beihang University, Beijing 100191, China

2. Unmanned Aerial Vehicle Research Institute, Beihang University, Beijing 100191, China)

Abstract: In this paper, we propose a hybrid approach based on the Lyapunov Guidance Vector Field (LGVF) and the Improved Interfered Fluid Dynamical System (IIFDS), to solve the problems of target tracking and obstacle avoidance in three-dimensional cooperative path planning for multiple unmanned aerial vehicles (UAVs). First, LGVF method is improved for UAV cooperative target tracking in 3D environment by introducing vertical component, with two guidance layers containing steering control and speed control. Second, IIFDS method is presented for UAVs to avoid obstacles or threats in complicated environment, where the local minimum problem is well resolved. Moreover, some cooperative strategies are added into the IIFDS framework to satisfy the constraints of obstacle avoidance and cluster maintenance. Finally, the missions of tracking target and avoiding obstacles can be performed simultaneously, by replacing the original sink fluid of IIFDS with the vector field of LGVF. Besides, the reactive parameters of IIFDS can be adjusted by the rolling optimization strategy to enhance the path quality. The experimental results validate the effectiveness of the hybrid method.

Keywords: Lyapunov Guidance Vector Field (LGVF); Improved Interfered Fluid Dynamical System (IIFDS); unmanned aerial vehicles (UAVs); three-dimensional cooperative path planning; the rolling optimization strategy

1 Introduction

In the last few decades, the unmanned aerial vehicles (UAVs) have been widely utilized in military or civilian fields e.g. surveillance, reconnaissance, search and rescue operations. The increasing demands have brought in the focus on enhancing the intelligence and autonomy of UAVs. Autonomous path planning is one of the critical UAV technologies to reduce dependencies on human operators [1-3]. Compared to the simple two-dimensional (2D) path, a three-dimensional (3D) route is more effective in improving UAV capabilities of low-altitude penetration and terrain following. Besides, multiple UAVs can carry out tasks more efficiently than single UAV. The 3D cooperative path planning problem, with applications to target tracking and obstacle avoidance simultaneously in a complicated and dynamic environment, is hence studied in this paper.

Target tracking is a complicated problem involving in multi-sensor information fusion, image processing, control technology, etc. And it is regarded as a path planning problem in this paper, assuming the target motion to be known. If there is only one UAV performing the task of target tracking, the target will flee easily from the field of view (FOV) of camera, which is a small circular region and cannot cover the whole planning space. But team tracking will improve the sensor coverage by sharing information between UAVs. In previous works, many motion planning methods have been proposed for cooperative target tracking. For the collaborative tracking task in urban environments, Shaferman et al. [4] model the restricted region, sensor coverage region and visibility area, and utilize the co-evolution genetic algorithm (CEGA) to optimize the tracking performance of UAVs. In Ref [5], rendezvous and standoff target tracking is solved by using the differential geometry, with the advantages of explicit use of a target velocity, rigorous stability and tuning parameter reduction. The nonlinear model predictive control method with fully decentralized controller structure is presented to get the optimal performance of standoff tracking for multiple UAVs [6]. The dynamic programming method is adopted to minimize the distance error covariance but it ignores the relative angle in Ref [7]. Frew et al. [8] propose the Lyapunov Guidance Vector Field (LGVF) for two-UAV standoff target tracking. In the decoupled guidance structure, heading-rate and speed are controlled respectively for the convergence to standoff distance and uniform phase distribution. To make UAV converge to standoff circle along the shortest route, Chen et al. [9] propose the tangent guidance vector field (TGVF), but this method fails when UAV is inside of the limit cycle. Hence the LGVF and TGVF method are adopted separately when UAV is inside or outside of the expected limit cycle in Ref [10]. Besides, there are other algorithms utilized in this area e.g. the Helmsman behavior, controlled collective motion, backstepping theory, partially observable Markov decision

*Corresponding author. Tel.: +86-10-82317546.
E-mail address: whl_gx_d102@163.com

processes (POMDP) [11,12,13]. But the above methods are only effective to 2D target tracking. What's more, UAVs often fly in a complicated environment, meaning that there are obstacles or threats (e.g. hills, buildings or radars) UAVs may crash into. But most methods ignore the case, or just adopt simple behaviors of obstacle avoidance while assuming the environment to be simple.

Aiming at the problem of obstacle avoidance in complicated environment, the environment constraints and UAV performance constraints (e.g. maximum or minimum velocity, maximum turn rate and maximum flight-path angle) should be considered, which can complicate the solution. Many studies are carried out in past decades concentrating on the collaborative framework, the path computation efficiency and path quality. Model Predicted Control (MPC) method [14], Voronoi method [15], intelligent algorithms (e.g. Genetic Algorithm, Particle Swarm Optimization) [2,3,16,17], Rapidly-exploring Random Tree (RRT) method [18], and Artificial Potential Field (APF) [19] are some of typical algorithms. In Ref [20], the so-called Feedback Based Compositional Rule of Inference (FBCRI) is proposed to solve the cooperative path planning problem, by embedding the feedback mechanism into the optimal fuzzy reasoning method. Zhang et al. [21] present the Cooperative and Geometric Learning Algorithm (CGLA) to solve the problems of collision avoidance and information sharing. By real-timely updating the individual cost matrix, weight matrix and risk evaluation, collision-free paths of multiple UAVs can be obtained. In Ref [22], the researchers adopt a novel hybrid model and develop the so-called neuro-dynamic programming (NDP) algorithm to guide UAVs avoid obstacles. However, to the best of our knowledge, the abovementioned methods are more efficient in planning 2D paths, while the computation quantity will increase explosively in 3D complex environment. Besides, the smoothness of paths may be unsatisfactory, so these preliminary paths have to be further mended by some smoothing strategies. On the basis of above consideration, the Interfered Fluid Dynamical System (IFDS) method is proposed in our previous work [23-24] for one UAV to plan the safe and smooth path, by imitating the phenomenon of fluid flowing. IFDS has the advantages of high computation efficiency and good path quality. However, the problem of local minimum exists and UAV cannot escape from the concave region or stagnation point sometimes. Besides, in order to apply IFDS to multi-UAV path planning, some other strategies should be added into the method.

The actual flight environment of UAVs is usually very complicated, where in many cases UAVs should avoid various obstacles and track target at the same time. However, it can be concluded from the above analysis that most path planning methods cannot compromise between these two tactical requirements, especially in 3D dynamic complicated environment. Besides, the computation efficiency and path quality are still unsatisfactory. In our previous work [25], a hybrid method combing LGVF and IFDS has been proposed for one-UAV path planning, but there are still some drawbacks. Hence we improve these two methods for multi-UAV path planning in this paper, and then combine the Lyapunov Guidance Vector Field (LGVF) and the Improved Interfered Fluid Dynamical System (IIFDS). First, LGVF is utilized for target tracking, and the height component is added into the traditional Lyapunov distance function for the convergence to optimal height, with no influence on the convergence to uniform phase distribution on the limit cycle. Second, IIFDS method is proposed by introducing the tangential matrix into the modulation matrix of IFDS, and it can solve the local minimum problem effectively. Some collaborative strategies including virtual obstacle and extra-attraction fluid are separately presented to satisfy the spacing constraints of multiple UAVs. Eventually, the missions of target tracking and obstacle avoidance can be well achieved simultaneously, by regarding the vector field from LGVF as the initial sink fluid of IIFDS. Besides, the reactive parameters of IIFDS should be adjusted in rolling horizon to enhance the path quality.

The remaining paper is organized as follows. Section 2 models the problem of path planning. In Section 3, the cooperative target tracking by LGVF is described. In Section 4, obstacle avoidance for multi-UAVs by IIFDS is introduced. In Section 5, the combination of two methods and the rolling optimization strategy are described. The simulation results are analyzed in Section 6. Section 7 concludes the paper.

2. Modeling of path planning

2. 1 Problem Description

In this paper, multiple UAVs perform the missions of tracking moving target and avoiding obstacles simultaneously in the complex and dynamic environment. An effective target tracking method should be proposed to enhance the

surveillance and reconnaissance ability of UAVs. Besides, there are dense static obstacles and moving threats in the planning space, so UAVs should avoid them safely during the process of target tracking. In addition, collision avoidance and cluster maintenance between UAVs should be considered for cooperative mechanism. To ensure the feasibility of path, the planned path should meet UAV dynamic constraint. Overall, the cooperative path planning problem is actually an optimization problem under various constraints. The discrete waypoints satisfying the certain optimization indexes under constraints should be generated quickly, and the planned path is finally obtained by connecting them.

2.2 Modeling of UAV

In this paper, UAV can be simplified as a typical three-degree-of-freedom (3-DOF) point-mass model with a stable low-level flight control system (FCS). The kinematic model in the inertial reference frame o_xyz can be described as:

$$\begin{cases} \dot{x} = V\cos\gamma\cos\psi \\ \dot{y} = V\cos\gamma\sin\psi \\ \dot{z} = V\sin\gamma \\ \dot{\psi} = \omega \end{cases} \tag{1}$$

where $P=(x,y,z)$ is the 3D position of UAV, $(u_x,u_y,u_z)=(\dot{x},\dot{y},\dot{z})$ the velocity of UAV, V the air speed, γ the flight path angle, ψ the heading angle, ω the turn rate. To make the LGVF method in Section 3 easier to understand, we define the horizontal air speed as $v = V\cos\gamma$. UAV model can hence be redefined as:

$$\begin{cases} \dot{x} = v\cos\psi \\ \dot{y} = v\sin\psi \\ \dot{z} = v\tan\gamma \\ \dot{\psi} = \omega \end{cases} \tag{2}$$

To ensure the feasibility of planned path, the state variables of any waypoint $P_k=(x_k,y_k,z_k)\ \forall k=1,2,\ldots,K$ should satisfy the following dynamic constraints:

$$\begin{cases} \left|\psi_{k+1}-\psi_k\right| \le \omega_{\max}\cdot\Delta T \\ \gamma_{\min} \le \gamma_k \le \gamma_{\max} \\ v_{\min} \le v_k \le v_{\max} \\ h_{\min} \le z_k \le h_{\max} \end{cases} \tag{3}$$

where $\omega_{\max}$ is the maximum UAV turn rate, ΔT the sampling time, $\gamma_{\min}$ and $\gamma_{\max}$ the minimum and maximum flight path angle, $v_{\min}$ and $v_{\max}$ the minimum and maximum air speed, $h_{\min}$ and $h_{\max}$ the minimum and maximum altitude. Further, by fully considering UAV kinematics and dynamics model, the method called trajectory propagation can be utilized to judge the feasibility of path. The details can be obtained from our previous work [26]. In addition, one UAV only detects the underneath circle area with radius R_r i.e. $S_P=\{P\,|\,\sqrt{(x-x_k)^2+(y-y_k)^2}\le R_r\}$, but UAVs can share information with each other to broaden the detecting coverage.

Multiple UAVs may collide with each other if they are too close. Hence the path should satisfy the constraint-that the distance between any two UAVs should be larger than the desired minimum distance d_{safe}. Communication is the foundation of cooperative framework, and UAVs can only exchange information with UAVs which are within the distance range of communication. The fully connected communication topology is utilized in this paper, meaning that the distance between any two UAVs should be smaller than the desired maximum distance d_{inf}. The abovementioned spacing constraint concept is illustrated in Fig. 1, where the dotted lines denote the boundaries of path, and d is the distance between two UAVs. Hence this bound can be simply modeled as $d_{\text{safe}} \le d \le d_{\text{inf}}$. Only two UAVs are described in this figure, but it can extend to the case of multiple UAVs.

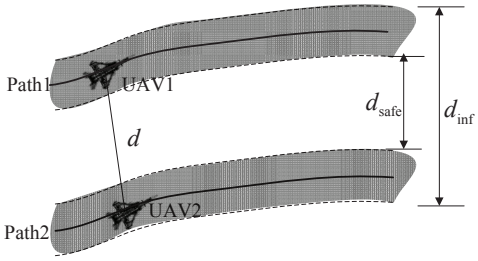

Fig. 1 Spacing constraint of multiple UAVs

Suppose that multiple UAVs perform tasks in the environment, named as UAV1, UAV2, etc. For the cooperative path planning, there will be couplings between the behaviors of multi-UAVs for each other, which may even lead to the failure of planning. Therefore we define UAV1 as the leader and assume other UAVs as the followers. Then each UAV performs the one-way behaviors of collision avoidance and cluster maintenance orderly, which will be described detailedly in Section 4.2.

2.3 Modeling of Target

We define the 3D inertial position of target as $P_t=(x_t,y_t,z_t)$ and the velocity of target as $(u_{tx},u_{ty},u_{tz})=(\dot{x}_t,\dot{y}_t,\dot{z}_t)$. If the target speed is larger than UAV maximum speed, the target may flee away from the FOV of UAV, and then UAV will not catch up with target. Consequently, the current information of target will be lost, leading to the failure of mission. Hence we assume that the target speed is always less than v_{max}. In this paper, the acceleration speed of target is assumed to be variable. The state equation and observation equation can be expressed as follows:

$$\begin{cases} \boldsymbol{X}_{k+1}=\boldsymbol{f}(\boldsymbol{X}_k)+\boldsymbol{w}_k \\ \boldsymbol{Z}_{k+1}=\boldsymbol{h}(\boldsymbol{X}_k)+\boldsymbol{v}_k \end{cases} \tag{4}$$

where $\boldsymbol{X}_k=[x_t,y_t,z_t,\dot{x}_t,\dot{y}_t,\dot{z}_t]^T$ is the motion state; $\boldsymbol{Z}_k=[x_t,y_t,z_t]^T$ is the observed value; $\boldsymbol{f}$ and $\boldsymbol{h}$ are the state equation and observation equation; $\boldsymbol{w}_k$ and $\boldsymbol{v}_k$ are the zero-mean Gaussian process noise and observation noise i.e. $p(\boldsymbol{w})\sim N(0,\boldsymbol{Q})$ and $p(\boldsymbol{v})\sim N(0,\boldsymbol{R})$, where $\boldsymbol{Q}$ and $\boldsymbol{R}$ are the corresponding covariance matrixes. The traditional Kalman Filter does not apply to state prediction of nonlinear system, so Extended Kalman Filter (EKF) is utilized to predict the future motion of target [27].

The target reference frame $P_t\_x_ty_tz_t$ can be defined by taking the target position as the origin of frame, where the moving target is relatively static. The illustrations of inertial reference frame and target reference frame are shown in Fig. 2. In this figure, $r=\sqrt{x_r^2+y_r^2}=\sqrt{(x-x_t)^2+(y-y_t)^2}$ is the distance between UAV and target in horizontal plane, and $h=z_r=z-z_t$ is the vertical distance.

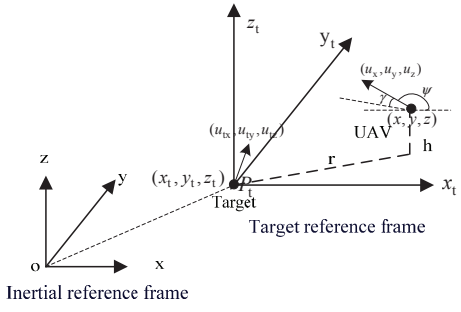

Fig. 2 Illustration of reference frames

The standoff target tracking problem is studied in this paper. According to Ref [8], UAVs should converge to the desired limit cycle above the target and be distributed uniformly in phase. The standoff distance R is taken as the radius of limit cycle, and the optimal height H is taken as the height of limit cycle. The values of R and H are usually influenced by many factors, e.g. the detection capabilities of onboard camera, the maneuvering capability of UAVs, the complexity of terrain environment and etc. In this paper, we assume that R and H are already known in advance.

2.4 Environment Modeling

In real flight environment, UAV is obliged to avoid obstacles during the process of target tracking. There are many kinds of obstacles, e.g. mountains, buildings, radars and etc. The obstacles or threats can be modeled by many methods e.g. Catmull-Rom surface, probabilistic risk by normal distribution function [21, 28]. In this paper, the following function is adopted to simplify the model of obstacle or threat:

$$\Gamma = (\frac{x-x_0}{a})^{2p} + (\frac{y-y_0}{b})^{2q} + (\frac{z-z_0}{c})^{2r} \tag{5}$$

where a,b,c are the size parameters, p,q,r the shape parameters, (x_0, y_0, z_0) the position of the obstacle center. By choosing different parameters, we can obtain various kinds of obstacles, e.g. sphere, cylinder, as shown in Fig. 3. $\Gamma = 1$ means the surface of obstacle; $\Gamma < 1$ is the danger area i.e. the region inside of the obstacle; $\Gamma > 1$ refers to the safe area i.e. the region outside of the obstacle. If UAV is too close to the obstacle surface, however, UAV cannot avoid it reactively in according to the maneuverability limitation. For the safety, the dilatation parameter λ_d (greater than 1) is hence proposed to virtually enlarge the size of obstacle. The value of λ_d can be determined by the cut-and-trial method, considering both UAV maneuverability and obstacle data. In addition, the velocity of moving threat is assumed to be less than that of UAV in this paper.

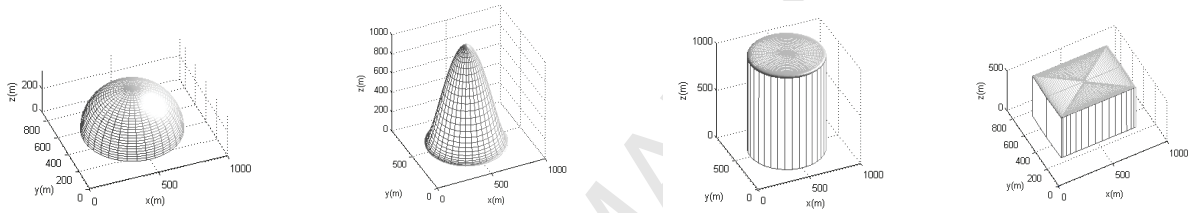

(a)sphere($a=b=c, p=q=r=1$) (b)cone ($a=b, p=1, q=1, r<1$) (c) cylinder ($a=b, p=1, q=1, r>1$) (d) cuboid ($p>1, q>1, r>1$)

Fig. 3 Approximation of typical obstacles

3. Cooperative Target Tracking by LGVF

In Ref [8], LGVF is utilized for 2D stand-off target tracking. The guidance layer consists of two steps i.e. steering control and speed control respectively. In the first step, the turn rate of individual UAV inferred from the Lyapunov distance function can guide UAV to converge to the desired limit cycle above the moving target. In the second step, the speeds of all UAVs are adjusted based on the Lyapunov phase function, making UAVs distribute uniformly in phase on the limit cycle eventually. For the mission of tracking target in 3D space, the height component should be taken into consideration. In our previous work [25], LGVF method has been improved for the mission by one UAV. In this paper, we will solve the problem of cooperative tracking by adjusting the speed of each UAV on the basis of [25], which will be described in Section 3.2.

3.1 Target Tracking by One UAV

Suppose that UAV is tracking a static ground target $P_t = (x_t, y_t, z_t)$ with the constant horizontal speed v_0 ($v_{min} \le v_0 \le v_{max}$). The Lyapunov distance function can be expressed as follows:

$$V_d = \frac{1}{2}(r^2 - R^2)^2 + \frac{1}{2}(h^2 - H^2)^2 \tag{6}$$

Based on Eq. (6), the guidance vector field can be inferred, where the desired velocity $\boldsymbol{u}$ is given as follows:

$$\boldsymbol{u} = \begin{bmatrix} u_x \\ u_y \\ u_z \end{bmatrix} = \frac{v_0}{r \cdot (r^2 + R^2)} \begin{bmatrix} -x_r \cdot (r^2 - R^2) - y_r \cdot (2rR) \\ -y_r \cdot (r^2 - R^2) + x_r \cdot (2rR) \\ -\lambda \cdot r \cdot (h^2 - H^2) \end{bmatrix} \tag{7}$$

where λ determines the rate of convergence to optimal height, and it is noticed that the horizontal speed is equal to v_0. Then we can infer:

$$\frac{dV_d}{dt}=\left[\frac{\partial V_d}{\partial x},\frac{\partial V_d}{\partial y},\frac{\partial V_d}{\partial z}\right]\cdot\begin{bmatrix}u_x\\u_y\\u_z\end{bmatrix}=\frac{-2rv_0\cdot(r^2-R^2)^2-2\lambda v_0\cdot(h^2-H^2)^2}{r^2+R^2} \tag{8}$$

The inequation $dV_d/dt\le 0$ always holds, and dV_d/dt is equal to 0 when UAV is on the limit cycle with the optimal height i.e. $r=R$ and $h=H$. On the basis of the Lasalle invariance principle, the velocity $\boldsymbol{u}$ will guide UAV converge to this stable region. Then we obtain the desired heading angle $\psi=\arctan(u_y/u_x)$, and the turn rate is inferred to be $\dot{\psi}=4v_0\cdot\frac{Rr^2}{(r^2+R^2)^2}$, and then we can compute the maximum value i.e. $\dot{\psi}_{\max}=v_0/R$. To ensure the feasibility of path, the condition $v_0/R\le\omega_{\max}$ i.e. $R\ge v_0/\omega_{\max}$ should be fulfilled. The flight path angle is $\gamma=\arctan(\frac{u_z}{v_0})=\arctan(\frac{-\lambda\cdot(h^2-H^2)}{r^2+R^2})$, with the range of $C_\gamma=\left[\arctan(\frac{-\lambda\cdot({h_{\max}}^2-H^2)}{R^2}),\arctan(\frac{-\lambda\cdot({h_{\min}}^2-H^2)}{R^2})\right]$. To guarantee the feasibility of path, $C_\gamma\subset[\gamma_{\min},\gamma_{\max}]$ should hold. Hence we infer $0<\lambda\le\min\left\{\frac{-\tan\gamma_{\min}\cdot R^2}{({h_{\max}}^2-H^2)},\frac{-\tan\gamma_{\max}\cdot R^2}{({h_{\min}}^2-H^2)}\right\}$.

If there is a moving ground target with velocity $\boldsymbol{u}_t=[u_{tx},u_{ty},0]^T$, the relative Lyapunov guidance vector field can be redefined as:

$$\boldsymbol{u}(P)=\begin{bmatrix}\alpha u_x\\\alpha u_y\\u_z\end{bmatrix}+\begin{bmatrix}u_{tx}\\u_{ty}\\0\end{bmatrix} \tag{9}$$

where α is the horizontal speed correction coefficient. It can be obtained by resolving the following equation to make the horizontal speed remain constant v_0:

$$(u_x^2+u_y^2)\cdot\alpha^2+2(u_xu_{tx}+u_yu_{ty})\cdot\alpha+u_{tx}^2+u_{ty}^2-{v_0}^2=0 \tag{10}$$

As the speed of target is always less than that of UAV, there must be a positive solution. Then we can infer:

$$\frac{dV_d}{dt}=\frac{-2\alpha rv_0\cdot(r^2-R^2)^2-2\lambda v_0\cdot(h^2-H^2)^2}{r^2+R^2}\le 0 \tag{11}$$

Therefore UAV can still converge to the limit cycle with the optimal height in the target reference frame, and the velocity of UAV relative to target is $[\alpha u_x,\alpha u_y,u_z]^T$. Fig. 4 describes the process of tracking a moving target in the inertial reference frame and the target reference frame respectively [25]. Next we analyze the feasibility of path. The heading angle is $\psi=\arctan(\frac{\alpha u_y+u_{ty}}{\alpha u_x+u_{tx}})$, and the turn rate can be inferred to meet $\dot{\psi}\le 4(\alpha^2+\alpha)v_0\cdot\frac{Rr^2}{(r^2+R^2)^2}$. Hence we can infer $R\ge\frac{v_0\cdot(\alpha^2+\alpha)}{\omega_{\max}}$. As we assume that the target only moves in horizontal plane, the value range of λ is the same as that of tracking static target.

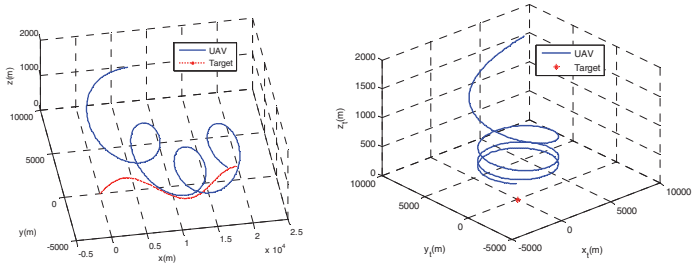

(a) Inertial reference frame (b)Target reference frame

Fig. 4 Tracking a moving target by one UAV

3.2 Target Tracking by Multiple UAVs

The camera, installed on UAV, could detect the battlefield environment. The motion information of target can be obtained, if the target is in the field of view (FOV) of camera. However，the FOV range of camera is usually limited with some blind spots. Compared to single UAV, a team of UAVs will improve the sensor coverage. As long as the target is in the FOV of one UAV, will the target be detected. The superiority of multiple UAVs will be particularly evident when the target is uncooperative or agile, in which case the motion information is hard to obtain and predict.

In this paper UAVs should be distributed uniformly in phase on the limit cycle [8]. The phase coordination is achieved by adjusting v_0 i.e. the horizontal speeds of UAVs. It is noticed that this adjustment will have no influence on the heading angles, meaning that UAVs will not deviate from the limit cycle.

Suppose there are $N_u\left(N_u \geq 2\right)$ UAVs in the flight environment. And the corresponding phase angle $\phi_i(i=1,2,\cdots,N_u)$ refers to the intersection angle between the *x* axis and the vector from target to UAV in horizontal plane. Fig. 5 illustrates the phase angles of three UAVs. The unwrapped difference between ϕ_1 and ϕ_2 should converge to ϕ_{D1}, and the unwrapped difference between ϕ_2 and ϕ_3 should converge to ϕ_{D2}, and so on. To distribute UAVs uniformly in phase, the phase differences of UAVs should be $\phi_{D1}=\phi_{D2}=\cdots=\phi_{D(N_u-1)}=\dfrac{2\pi}{N_u}$. The Lyapunov phase function can be defined as follows:

$$V_p=\frac{1}{2}(\phi_2-\phi_1-\phi_{D1})^2+\frac{1}{2}(\phi_3-\phi_2-\phi_{D2})^2+\cdots+\frac{1}{2}(\phi_{N_u}-\phi_{N_u-1}-\phi_{D(N_u-1)})^2 \tag{12}$$

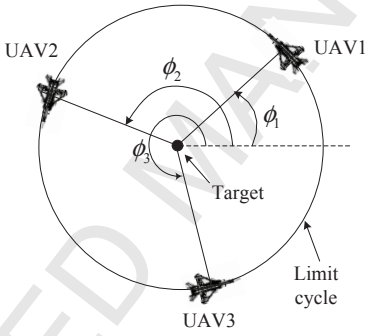

Fig. 5 Projection of three UAVs tracking target in horizontal plane

Then we obtain:

$$\frac{dV_p}{dt}=(\phi_2-\phi_1-\phi_{D1})(\dot{\phi}_2-\dot{\phi}_1)+\cdots+(\phi_{N_u}-\phi_{N_u-1}-\phi_{D(N_u-1)})(\dot{\phi}_{N_u}-\dot{\phi}_{N_u-1}) \tag{13}$$

To make the inequation $\dfrac{dV_p}{dt}\leq 0$ hold, we can define:

$$\begin{cases}\dot{\phi}_2-\dot{\phi}_1=-k_1(\phi_2-\phi_1-\phi_{D1})\\ \dot{\phi}_3-\dot{\phi}_2=-k_2(\phi_3-\phi_2-\phi_{D2})\\ \vdots\\ \dot{\phi}_{N_u}-\dot{\phi}_{N_u-1}=-k_{N_u-1}(\phi_{N_u}-\phi_{N_u-1}-\phi_{D(N_u-1)})\end{cases} \tag{14}$$

where $k_1,k_2,\cdots,k_{N_u-1}$ are positive values defining the convergence rate to the proper phase. We assume $\dot{\phi}_1=\dfrac{v_0}{R}$, then we can obtain other angular speeds of phase angles i.e. $\dot{\phi}_2,\ldots\dot{\phi}_{N_u}$ from the above equation.

Based on the above equation, $\phi_2-\phi_1$ will converge to ϕ_{D1}, and $\phi_3-\phi_2$ will converge to ϕ_{D2} eventually and so on. The horizontal air speeds of UAVs can be obtained as follows:

$$\begin{cases} v_1 = R\dot{\phi}_1 \\ v_2 = R\dot{\phi}_2 \\ \vdots \\ v_{N_u} = R\dot{\phi}_{N_u} \end{cases} \tag{15}$$

The phase angle is computed from the arc-tangent function, and the inequations $-\pi \le \phi_2 - \phi_1 - \phi_{D1} \le \pi$, $-\pi \le \phi_3 - \phi_2 - \phi_{D2} \le \pi$ hence hold, and so on. To ensure the feasibility of path, all the horizontal air speeds $v_1, v_2, \cdots, v_{N_u}$ should be within the speed limit $[v_{\min}, v_{\max}]$, so we can infer the ranges of $k_1, k_2, \cdots, k_{N_u-1}$ respectively. Then the speed by Eq.(15) can substitute v_0 in Eq.(7) respectively to determine the desired velocity of each UAV.

When the target is moving, the desired velocities of UAVs can be computed by Eq.(9). By choosing α from Eq.(10), the horizontal speeds will still be equal to $v_1, v_2, \cdots, v_{N_u}$ respectively in the inertial reference frame, which are within the speed limitation. Although the inequation $\frac{dV_p}{dt} \le 0$ holds in the inertial reference frame, this inequation may not hold in the target reference frame as the relative horizontal speeds are unequal to $v_1, v_2, \cdots, v_{N_u}$ any more. This will prevent UAVs converge to the desired phase spacing, causing vibration during the process of converging to the desired phase spacing.

4. Obstacle Avoidance by IIFDS

4.1 The description of IIFDS

In many cases, UAVs often need to fly at a low-altitude to avoid detection by enemy radars or infrared sensors. Consequently path planning for obstacle avoidance in 3D environment is essential, where a 3D safe path from the initial point to the destination is planned. Many methods have hence been proposed, but most of them are only applicable to 2D environment and the path quality is unsatisfactory. Therefore, the so-called IFDS method is proposed in our previous work [23-24]. By modifying the initial fluid with the modulation matrix, we will obtain the interfered fluid where the streamlines can be taken as planned paths. The procedures of IFDS can be seen in Ref [24].

The planned streamline by IFDS has proved to be impenetrable to obstacle, so the path will guide UAV avoid obstacles. The IFDS method, to certain degree, can be regarded as the extension of traditional Artificial Potential Field (APF). Similar to APF, the local minimum problem is the main drawback of IFDS [24]. For example, UAV may trap into the concave region produced by overlapping obstacles (the shadow area TA in Fig. 6(a)), or stop at the stagnation point (the point SP in Fig. 6(b)). In [24], we fill the concave area by virtual obstacles, or choose virtual destination to guide UAV escape TA or SP, but these strategies cannot solve the problem fundamentally.

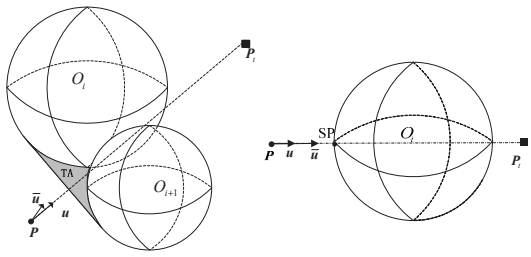

(a)Trap area (b) Stagnation point

Fig. 6 Local minimum problem

The primary cause of local minimum is that the definition of modulation matrix is not comprehensive, resulting in the limited distribution of streamlines. Hence IIFDS method is presented below, where the tangential matrix is introduced into the modulation matrix.

As shown in Fig. 7, for the w-th obstacle, two orthogonal tangent vectors can be chosen from the tangent plane which is perpendicular to the normal vector $\boldsymbol{n}_w = [\frac{\delta \Gamma_w}{\delta x}, \frac{\delta \Gamma_w}{\delta y}, \frac{\delta \Gamma_w}{\delta z}]^{\mathrm{T}}$:

$$\boldsymbol{t}_{w,1}=[\frac{\delta\Gamma_w}{\delta y},-\frac{\delta\Gamma_w}{\delta x},0]^{\mathrm{T}} \tag{16}$$

$$\boldsymbol{t}_{w,2}=[\frac{\delta\Gamma_w}{\delta x}\frac{\delta\Gamma_w}{\delta z},\frac{\delta\Gamma_w}{\delta y}\frac{\delta\Gamma_w}{\delta z},-(\frac{\delta\Gamma_w}{\delta x})^2-(\frac{\delta\Gamma_w}{\delta y})^2]^{\mathrm{T}} \tag{17}$$

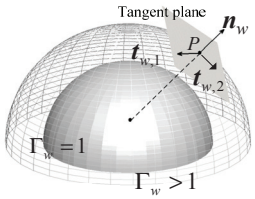

Fig. 7 Illustration of Vectors

Then the tangent reference frame o'-$x'y'z'$ is established by taking $\boldsymbol{t}_{w,1}$, $\boldsymbol{t}_{w,2}$ and $\boldsymbol{n}_w$ as the x' axis, y' axis and z' axis respectively. Hence any tangent vector from the tangent plane can be expressed as:

$$\boldsymbol{t}'_w=[\cos\theta_w,\sin\theta_w,0]^{\mathrm{T}} \tag{18}$$

where $\theta_w\in[-\pi,\pi]$ is called the tangential direction coefficient, which is the rotary angle along z' axis. Then in the inertial reference frame o-xyz, $\boldsymbol{t}'_w$ can be transformed to $\boldsymbol{t}_w$ as follows:

$$\boldsymbol{t}_w=\boldsymbol{R}_w\boldsymbol{t}'_w \tag{19}$$

where $\boldsymbol{R}_w$ is the coordinate transformation matrix from o'-$x'y'z'$ to o-xyz

We can define the modulation matrix of the w-th obstacle as follows:

$$\boldsymbol{M}_w=\boldsymbol{I}-\frac{\boldsymbol{n}_w\boldsymbol{n}_w^{\mathrm{T}}}{|\Gamma_w|^{\frac{1}{\rho_w}}\boldsymbol{n}_w^{\mathrm{T}}\boldsymbol{n}_w}+\frac{\boldsymbol{t}_w\boldsymbol{n}_w^{\mathrm{T}}}{|\Gamma_w|^{\frac{1}{\sigma_w}}\|\boldsymbol{t}_w\|\|\boldsymbol{n}_w\|} \tag{20}$$

where ρ_w is the repulsive reaction coefficient and σ_w is the tangential reaction coefficient. The first part of $\boldsymbol{M}_w$ i.e. the unit matrix $\boldsymbol{I}$ can be called the attractive matrix, the second part the repulsive matrix, the third part the tangential matrix.

The other procedures of IIFDS are the same those of IFDS. The pseudo code of IIFDS is shown in Table 1.

Table.1. Pseudo code of IIFDS

Obstacle avoidance based on IIFDS
1. **while** (mission uncompleted)
2. Take the sink fluid as the initial fluid, whose velocity is $\boldsymbol{u}=-\left[\frac{v_0(x-x_t)}{d(P,P_t)},\frac{v_0(y-y_t)}{d(P,P_t)},\frac{v_0(z-z_t)}{d(P,P_t)}\right]^{\mathrm{T}}$
3. Update the information of obstacles or threats: model function Γ_w, velocity $\boldsymbol{v}_w$, $w\in 1...W$
4. **for** each obstacle, calculate
5. The weighting coefficient $\omega_w=\begin{cases}1 & W=1\\ \prod_{i=1,i\neq w}^{W}\frac{(\Gamma_i-1)}{(\Gamma_i-1)+(\Gamma_w-1)} & W\neq 1\end{cases}$
6. The tangent vector by Eqs. (16-19)
7. The modulation matrix by Eqs. (20)
8. **end for**
9. The overall modulation matrix $\bar{\boldsymbol{M}}=\sum_{w=1}^{W}\omega_w\boldsymbol{M}_w$
10. The overall velocity of threats $\boldsymbol{v}=\sum_{w=1}^{W}\omega_w\exp(\frac{-\Gamma_w}{\lambda_w})\boldsymbol{v}_w$
11. The disturbed fluid velocity $\bar{\boldsymbol{u}}=\bar{\boldsymbol{M}}(\boldsymbol{u}-\boldsymbol{v})+\boldsymbol{v}$
12. The next waypoint $P_{k+1}=P_k+\bar{\boldsymbol{u}}\cdot\Delta T$
13. **end while**

When UAV is on the surface of the w-th obstacle i.e. $\Gamma_w=1$, the weighting coefficients satisfy $\omega_w=1$, $\omega_i=0\,(i=1\cdots W,\ i\neq w)$. Hence the overall modulation matrix will be $\bar{\boldsymbol{M}}=\boldsymbol{M}_w=\boldsymbol{I}-\frac{\boldsymbol{n}_w\boldsymbol{n}_w^{\mathrm{T}}}{\boldsymbol{n}_w^{\mathrm{T}}\boldsymbol{n}_w}+\frac{\boldsymbol{t}_w\boldsymbol{n}_w^{\mathrm{T}}}{\|\boldsymbol{t}_w\|\|\boldsymbol{n}_w\|}$. As the tangent vector $\boldsymbol{t}_w$ and the normal vector $\boldsymbol{n}_w$ are perpendicular i.e. $\boldsymbol{n}_w^{\mathrm{T}}\boldsymbol{t}_w=0$, we can infer $\boldsymbol{n}_w^{\mathrm{T}}(\bar{\boldsymbol{u}}-\boldsymbol{v})=\boldsymbol{n}_w^{\mathrm{T}}\boldsymbol{M}_w(\boldsymbol{u}-\boldsymbol{v})=0$, meaning that the radial component of $\bar{\boldsymbol{u}}-\boldsymbol{v}$ is 0. Hence UAV will not penetrate into the obstacle or threat.

By utilizing the traditional IFDS method, the disturbed velocity can only be decomposed into attractive velocity and repulsive velocity. With different parameters, the streamlines can only distribute in a plane and hence UAV will easily trap into TA. In a word, IFDS is a pseudo-3D method. Compared to IFDS, the tangential velocity is added into the disturbed velocity by the IIFDS method. By adjusting parameters ρ_w, σ_w or θ_w, we can obtain the streamlines distributing in the whole 3D space, from which the route without local minimum can be easily chosen. But it should be noticed that the value of θ_w needs to ensure the three velocity components to be not coplanar. If the three velocity components are coplanar, all the streamlines with different parameters will only distribute in a plane. Besides, it should be noticed that the bigger ρ_w or σ_w is, the earlier and more drastically the path avoids obstacle.

4.2 The collaborative strategies

When there are multiple UAVs in the environment, each UAV can avoid obstacles separately by the IIFDS method. Then, to satisfy the constraints of collision avoidance and communication maintenance, some collaborative strategies are introduced into the framework of IIFDS.

4.2.1 Collision Avoidance

The "virtual obstacle" strategy is utilized here to resolve the problem of collision avoidance. Suppose there are one leader UAV1 and some followers UAV2, UAV3, etc. The leader UAV needs not consider other UAVs as virtual obstacles, and the desired velocity $\bar{\boldsymbol{u}}_1$ can be calculated by IIFDS directly. For path planning of UAV2, we should take UAV1 as the virtual sphere threat with radius d_{safe} and velocity $\bar{\boldsymbol{u}}_1$. Then its disturbed velocity $\bar{\boldsymbol{u}}_2$ can be computed by IIFDS method. For UAV3, both UAV1 and UAV2 should be taken as virtual sphere threats with the radius d_{safe} and the velocity $\bar{\boldsymbol{u}}_1$ or $\bar{\boldsymbol{u}}_2$ separately. The procedures for other UAVs are the same as the above-mentioned strategies. It has been proved in Section 4.1 that the path by IIFDS can avoid obstacles or threats, so the collision between UAVs will be avoided.

4.2.2 Maintenance of Cluster

The maintenance of cluster means that the distance between UAVs should be less than the maximum distance. When UAVs fly in a cluster, they can keep communication with each other. First we utilize the hyperbolic tangent function to convert the distance to a value between 0 and 1:

$$f(d, d_{\text{inf}}, \Delta d) = \frac{1}{2}\left[1 + \tanh\left(\frac{d - d_{\text{inf}} + \frac{\Delta d}{2}}{\frac{\Delta d}{8}}\right)\right] \tag{21}$$

where $0 < \Delta d \ll d_{\text{inf}}$. This function is derivable globally with the following properties: when $d \geq d_{\text{inf}}$, then $f \to 1$; when $d \leq d_{\text{inf}} - \Delta d$, then $f \to 0$; when $d_{\text{inf}} - \Delta d \leq d \leq d_{\text{inf}}$, f increases with fast transitions. The shape of f is shown in Fig. 8.

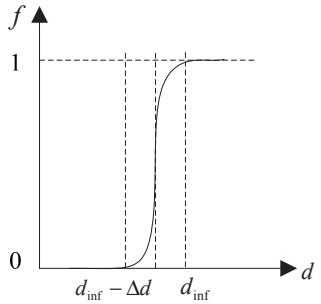

Fig. 8 Shape of function f

Like Section 4.2.1, the following strategies will not be performed for UAV1. Then we describe the strategy for UAVi($i \geq 2$).

First the distance between UAVi and UAV$j\left(j=1,\cdots,i-1\right)$ is computed by $d_{ij}=\sqrt{(x_i-x_j)^2+(y_i-y_j)^2+(z_i-z_j)^2}$, where (x_i,y_i,z_i) and (x_j,y_j,z_j) are the positions of UAVi and UAVj respectively. Then we obtain f_{ij} by Eq. (21). The weighing coefficient w_{ij} of UAVj will be obtained:

$$w_{ij}=\begin{cases}1 & i=2\\ \prod\limits_{k=1,k\neq j}^{i-1}\dfrac{(1-f_{ik})}{(1-f_{ik})+(1-f_{ij})} & i>2\end{cases} \tag{22}$$

The attractive velocity from UAVi to UAVj is:

$$\boldsymbol{u}_{ij}=-\left[\frac{v_0(x_i-x_j)}{d_{ij}},\frac{v_0(y_i-y_j)}{d_{ij}},\frac{v_0(z_i-z_j)}{d_{ij}}\right]^{\mathrm{T}} \tag{23}$$

We presume that the velocity of UAV$j\left(j=1,\cdots,i-1\right)$ i.e. $\bar{\boldsymbol{u}}_j$ has been computed by IIFDS method. Then we can obtain the so-called extra-attraction fluid, the velocity of which is:

$$\boldsymbol{u}_a=\sum_{j=1}^{i-1}w_{ij}f_{ij}(\boldsymbol{u}_{ij}+\bar{\boldsymbol{u}}_j) \tag{24}$$

Then the initial fluid of IIFDS is defined, the velocity of which is:

$$\boldsymbol{u}=\boldsymbol{u}_a+(1-\sum_{j=1}^{i-1}w_{ij}f_{ij})\boldsymbol{u}_b \tag{25}$$

where $\boldsymbol{u}_b$ is the velocity of sink fluid from Table1. In this way, the initial fluid can be divided into two parts i.e. the sink fluid and the extra-attraction fluid. Eventually the desired velocity of UAVi is obtained by IIFDS method.

Theorem:

By introducing the extra-attraction fluid into the initial fluid, the distance between any two UAVs will always be less than desired maximum distance $d_{\inf}$.

Proof:

The disturbed velocity $\bar{\boldsymbol{u}}$ by IIFDS can be expressed as $\bar{\boldsymbol{u}}=\sum_{w=1}^{W}\omega_w\boldsymbol{M}_w\boldsymbol{u}=\sum_{w=1}^{W}\omega_w\bar{\boldsymbol{u}}_w$, where $\bar{\boldsymbol{u}}_w$ is generated as follows: $\bar{\boldsymbol{u}}_w=\boldsymbol{u}-\dfrac{\boldsymbol{n}_w^{\mathrm{T}}\boldsymbol{u}}{\left|\Gamma_w\right|^{\frac{1}{\rho_w}}\boldsymbol{n}_w^{\mathrm{T}}\boldsymbol{n}_w}\boldsymbol{n}_w+\dfrac{\boldsymbol{n}_w^{\mathrm{T}}\boldsymbol{u}}{\left|\Gamma_w\right|^{\frac{1}{\sigma_w}}\left\|\boldsymbol{t}_w\right\|\left\|\boldsymbol{n}_w\right\|}\boldsymbol{t}_w$. The velocity $\bar{\boldsymbol{u}}_w$ can be divided into three parts: $\boldsymbol{u}$ is the attractive velocity, $-\dfrac{\boldsymbol{n}_w^{\mathrm{T}}\boldsymbol{u}}{\left|\Gamma_w\right|^{\frac{1}{\rho_w}}\boldsymbol{n}_w^{\mathrm{T}}\boldsymbol{n}_w}\boldsymbol{n}_w$ the repulsive velocity, $\dfrac{\boldsymbol{n}_w^{\mathrm{T}}\boldsymbol{u}}{\left|\Gamma_w\right|^{\frac{1}{\sigma_w}}\left\|\boldsymbol{t}_w\right\|\left\|\boldsymbol{n}_w\right\|}\boldsymbol{t}_w$ the tangential velocity.

As is known, UAV can avoid obstacles by IIFDS method, so $\Gamma_w\geq 1$ holds. For the attractive and repulsive velocity, we can infer $\boldsymbol{u}^{\mathrm{T}}\left(\boldsymbol{u}-\dfrac{\boldsymbol{n}_w^{\mathrm{T}}\boldsymbol{u}}{\left|\Gamma_w\right|^{\frac{1}{\rho_w}}\boldsymbol{n}_w^{\mathrm{T}}\boldsymbol{n}_w}\boldsymbol{n}_w\right)=\left\|\boldsymbol{u}\right\|^2\left(1-\dfrac{\cos^2\left\langle\boldsymbol{u},\boldsymbol{n}_w\right\rangle}{\left|\Gamma_w\right|^{\frac{1}{\rho_w}}}\right)\geq 0$. For the tangential velocity, we can infer $\boldsymbol{u}^{\mathrm{T}}\left(\dfrac{\boldsymbol{n}_w^{\mathrm{T}}\boldsymbol{u}}{\left|\Gamma_w\right|^{\frac{1}{\sigma_w}}\left\|\boldsymbol{t}_w\right\|\left\|\boldsymbol{n}_w\right\|}\boldsymbol{t}_w\right)=\left\|\boldsymbol{u}\right\|^2\dfrac{\cos\left\langle\boldsymbol{u},\boldsymbol{n}_w\right\rangle\bullet\cos\left\langle\boldsymbol{u},\boldsymbol{t}_w\right\rangle}{\left|\Gamma_w\right|^{\frac{1}{\sigma_w}}}$. By choosing a proper tangential direction coefficient θ_w, the condition $\cos\left\langle\boldsymbol{u},\boldsymbol{n}_w\right\rangle\bullet\cos\left\langle\boldsymbol{u},\boldsymbol{t}_w\right\rangle\geq 0$ will hold. Hence we can infer $\boldsymbol{u}^{\mathrm{T}}\bar{\boldsymbol{u}}_w\geq 0$, and further obtain $\boldsymbol{u}^{\mathrm{T}}\bar{\boldsymbol{u}}=\sum_{w=1}^{W}\omega_w\boldsymbol{u}^{\mathrm{T}}\bar{\boldsymbol{u}}_w\geq 0$.

When the distance d_{ij} between UAVi and UAVj is equal to $d_{\inf}$, we will infer $f_{ij}=1$ and $w_{ij}=1$, $w_{kj}=0(k=1,...,j-1$ and $k\neq i)$. From Eqs.(24-25) we infer $\boldsymbol{u}=\boldsymbol{u}_{ij}+\bar{\boldsymbol{u}}_j$, meaning that only the extra-attraction fluid is taken into account. In consideration of the derived inequation $\boldsymbol{u}^{\mathrm{T}}\bar{\boldsymbol{u}}\geq 0$, d_{ij} will decrease. Therefore the inequation $d_{ij}\leq d_{\inf}$ always holds.

In this paper, the coordination strategies are achieved in IIFDS framework, so it has the advantages of high computation efficiency and good path quality compared to traditional methods.

5. Cooperative Target Tracking and Obstacle Avoidance

5.1 LGVF+IIFDS

The actual flight environment of UAVs is sometimes very complicated, where in many cases UAVs should avoid various obstacles and track target simultaneously under the collaborative mechanism. As the guidance vector fields by LGVF satisfy the fluid characteristics, they can replace the initial sink fluids of IIFDS. That is to say, the sink fluid velocity $\boldsymbol{u}_b$ in Eq.(25) can be replaced with the velocity generated by Eq.(9). It has been proved in Section 4.2.2 that IIFDS method can ensure the stability of fluid system i.e. $\boldsymbol{u}^{\mathrm{T}}\bar{\boldsymbol{u}} \geq 0$, so the velocities of the modified fluids by LGVF+IIFDS can guide UAVs track target and avoid obstacles well at the same time, with a proper spacing between any two UAVs. Based on this strategy, two methods can be combined skillfully and effectively.

The architecture of LGVF+IIFDS for three UAVs is illustrated in Fig. 9. First, the horizontal speeds of three UAVs, v_1, v_2, v_3, are obtained based on the Lyapunov phase function. Then the guidance vector fields with velocity $\boldsymbol{u}_1, \boldsymbol{u}_2, \boldsymbol{u}_3$ are calculated respectively from Lyapunov distance function. They are utilized as one part of initial fluid of IIFDS. The other part of initial fluid is the extra-attraction fluid by Eqs.(21-24), which can maintain the communication of UAVs. In addition, UAVs are taken as virtual obstacles, and the modulation matrix is then calculated based on the overall information of obstacles. By modulating the initial fluids with the modulation matrix, the interfered fluids with velocity $\bar{\boldsymbol{u}}_1, \bar{\boldsymbol{u}}_2, \bar{\boldsymbol{u}}_3$ are obtained separately. The paths of UAVs are finally obtained by the recursive integration of $\bar{\boldsymbol{u}}_1, \bar{\boldsymbol{u}}_2$ or $\bar{\boldsymbol{u}}_3$ respectively.

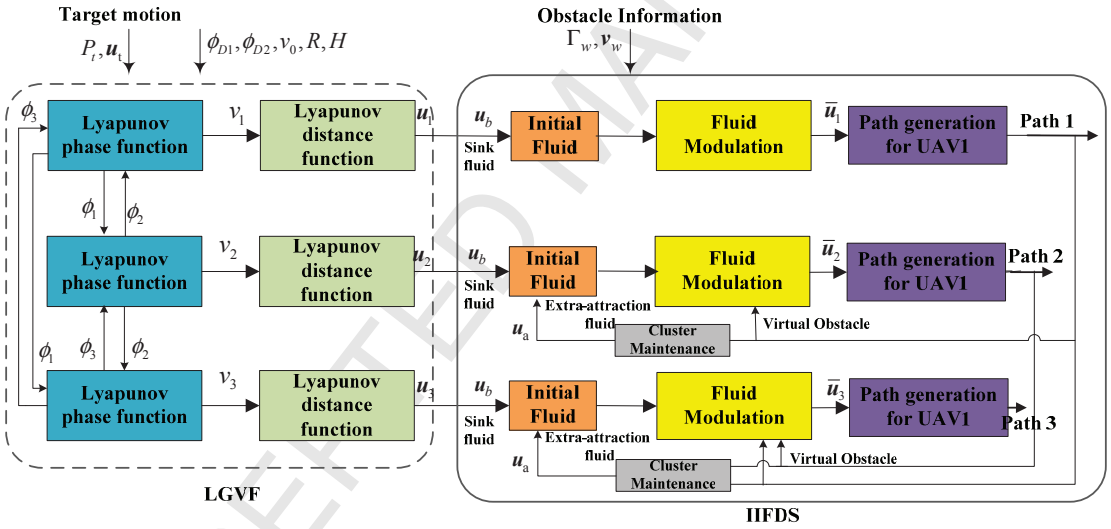

Fig. 9 Architecture of LGVF+IIFDS

5.2 Rolling optimization

The planned path by LGVF has proved to be feasible in Section 3, but the influence of obstacles will make the path by LGVF+IIFDS unfeasible sometimes. As the reactive parameters ρ_w, σ_w and θ_w have much influence on the path quality, the path quality can be enhanced by adjusting reactive parameters. Therefore, the rolling optimization strategy with centralized structure is utilized here to adjust the paths by LGVF+IIFDS, and the local paths will be confirmed ahead.

The illustration of rolling optimization strategy for three UAVs is displayed in Fig. 10. Suppose that three N-step paths $\{P_{1,k}, \cdots, P_{1,k+N}\}$, $\{P_{2,k}, \cdots, P_{2,k+N}\}$, $\{P_{3,k}, \cdots, P_{3,k+N}\}$ are planned ahead when the three UAVs arrive at $P_{1,k}$, $P_{2,k}$, $P_{3,k}$ separately at the time t_k. As the motion prediction results of target or threat will decrease with the increase of time domain, hence only the first path segment i.e. $P_{1,k}P_{1,k+1}$, $P_{2,k}P_{2,k+1}$ or $P_{3,k}P_{3,k+1}$ is executed by each UAV. During this execution process, the new optimal N-step paths by LGVF+IIFDS i.e. $\{P_{1,k+1}, \cdots, P_{1,k+N+1}\}, \{P_{2,k+1}, \cdots, P_{2,k+N+1}\}, \{P_{3,k+1}, \cdots, P_{3,k+N+1}\}$ are planned by adjusting reactive parameters. When the three UAVs arrive at $P_{1,k+1}$, $P_{2,k+1}$, $P_{3,k+1}$ separately at the time t_{k+1}, the

first step of each newly-planned route is then executed by each UAV. Repeat the above procedures until the mission is completed. It is noticed that, the time of local path planning should be less than the time of executing path (i.e. the sampling time ΔT).

The value of N is mainly influenced by the calculation time and the prediction accuracy. It can be determined by numerous Monte-Carlo simulations with different values of N in various scenarios.

The definition of optimizing index $J_i(k)$ for each UAV ($i=1,2,\cdots,N_u$) can be seen in Ref [25]. For multiple UAVs, the overall optimizing index $J(k)$ is obtained by $J(k)=\sum_{i=1}^{N_u} J_i(k)$.

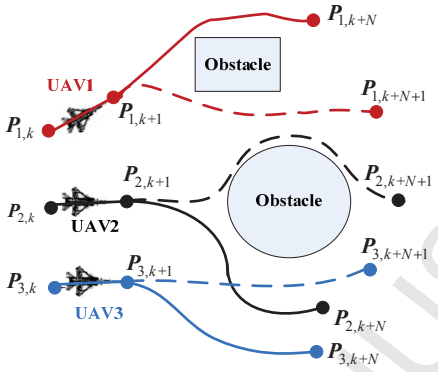

Fig. 10 Illustration of rolling optimization strategy

6. Simulation

The experiments are executed in MATALB R2011a on the computer with Intel Core i5 CPU processor and 2.5GHz frequency. The necessary parameters of path planning are listed in Table 2.

Table.2. Parameters of path planning

Parameter	Value
Sampling Time, ΔT (s)	1
Planning steps, N	5
Number of UAVs, N_u	3
Cruising velocity, v_0 (m/s)	50
Maximum UAV turn rate, $\omega_{\max}$ (deg/s)	30
Minimum/Maximum flight-path angle, $\gamma_{\min}$ (deg), $\gamma_{\max}$ (deg)	-30,30
Minimum/Maximum UAV altitude, $h_{\min}$ (m), $h_{\max}$ (m)	200,3000
Minimum/Maximum air speed, $v_{\min}$ (m/s), $v_{\max}$ (m/s)	30,70
Minimum/Maximum distance, d_{safe} (m), d_{inf} (m)	100,2000
Standoff distance, R (m)	500
Optimal height, H (m)	500
Coefficient of height convergence rate, λ	0.01
Coefficient of phase convergence rate, k_1 , k_2	0.005,0.008
Range of repulsive reaction coefficient, ρ_w	[0.1,5]
Range of tangential reaction coefficient, σ_w	[0.1,5]
Range of tangential direction coefficient, θ_w	$[-\pi,\pi]$
Detecting radius, R_r (m)	2000
Obstacle expansion parameter, λ_d	1.12

6.1. Cooperative target tracking by LGVF

Suppose that a target moves along an S-shape trajectory in the free environment with the start point $(1000,0,0)$m and the constant speed $v_t=20$m/s . Three UAVs perform the tasks of target tracking, and the start points are $(0,0,1000)$m , $(300,200,1500)$m and $(0,500,2000)$m respectively.

Fig. 11(a) illustrates the 3D paths of target tracking in the inertial reference frame. As readers only get little information from Fig. 11(a), the vertical information and the horizontal information of paths are shown in Fig. 11(b) and Fig. 11(c)

respectively. The heights of UAVs i.e. z will eventually converge to the optimal height H=500m . To illustrate the position relations of UAVs more clearly, Fig. 11(d) is provided to display the phase separations between UAVs, which vibrate around the desired phase spacing ($2\pi/3$) with a reasonable value. Further, Fig. 11(e) and Fig. 11(f) illustrate the process of target tracking in the target reference frame. It is obvious that all the three UAVs will converge to the limit cycle with radius R=500m and then fly on this cycle persistently. The simulation results indicate that the 3D cooperative target tracking mission is well resolved by LGVF method.

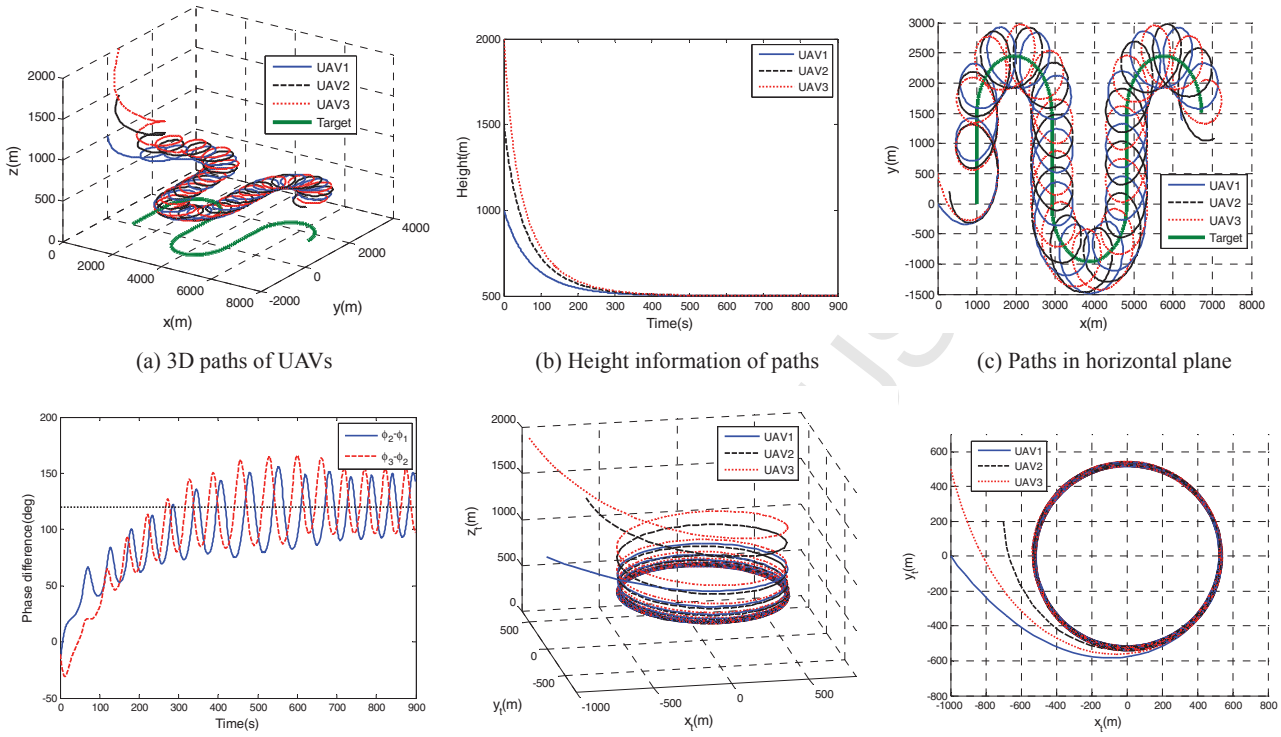

(a) 3D paths of UAVs (b) Height information of paths (c) Paths in horizontal plane

(d) Phase difference between UAVs (e) 3D paths of UAVs relative to target (f) Paths relative to target in horizontal plane

Fig. 11 Tracking a moving target by three UAVs

During the process of tracking a moving target, the phase difference between UAVs will try to achieve the desired phase spacing ($2\pi/3$). However, as discussed in Section 3.2, UAV airspeed limitations will prevent this convergence, causing the vibration of phase difference. Fig. 12 displays the phase separation between UAV2 and UAV3 i.e. $\phi_3-\phi_2$ versus different target speed v_t=0m/s , 5m/s, 10m/s, 20m/s separately. The amplitude of vibration is positively related to the target speed: the larger the target speed is, the greater the amplitude of vibration will be. If the target is static, the phase difference will converge to $2\pi/3$ smoothly without any vibration.

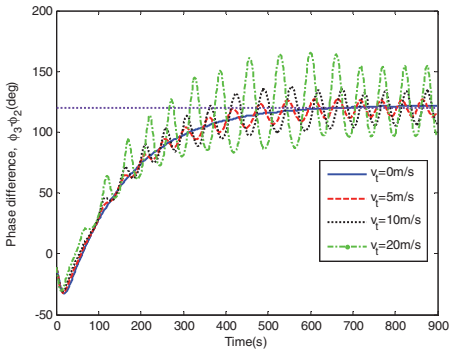

Fig. 12 Phase separation *vs* various target speeds

6.2. Comparison between paths by IFDS and IIFDS

Suppose there is a sphere static obstacle in the scenario, and only one UAV avoids this obstacle from the initial point

$[0,0,500]$m to the destination $[4000,4000,500]$m . The distribution of streamlines i.e. paths with different reactive parameters by IFDS is displayed in Fig. 13(a), where all the streamlines are only in a plane. The result by IIFDS is shown in Fig. 13(b), where the streamlines distribute much wider in the whole 3D planning space. Besides, the bigger the repulsive reaction coefficient ρ or the tangential reaction coefficient σ is, the earlier the streamline avoids obstacle with the larger disturbance amplitude. When the tangential direction coefficient θ approaches to 0, π or $-\pi$, there will be more horizontal component of streamline. If θ is closer to $\pi/2$, the path will have more vertical component.

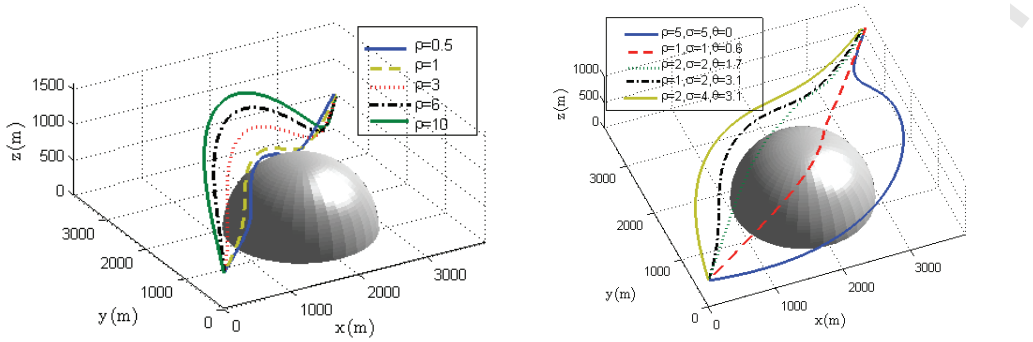

(a)IFDS (b) IIFDS

Fig. 13 Distribution of paths with different reactive parameters

Suppose there are five overlapping obstacles in the planning space, and the generated concave area is the trap area (TA), as shown in Fig. 14(a). The streamline by IFDS will be caught into TA. In Ref [24], the virtual obstacle (VO) is utilized to fill this concave region on the basis of IFDS. Although it can guide UAV avoid TA, the path smoothness is unsatisfactory. By utilizing the rolling optimization strategy to choose proper reactive parameters of IIFDS, the path by IIFDS can avoid this local minimum easily and smoothly. For the third obstacle, the optimal values of the tangential direction parameter during the whole process are illustrated in Fig. 14(b). As we see, the value of θ will be closer to $\pi/2$ when UAV is in the concave area.

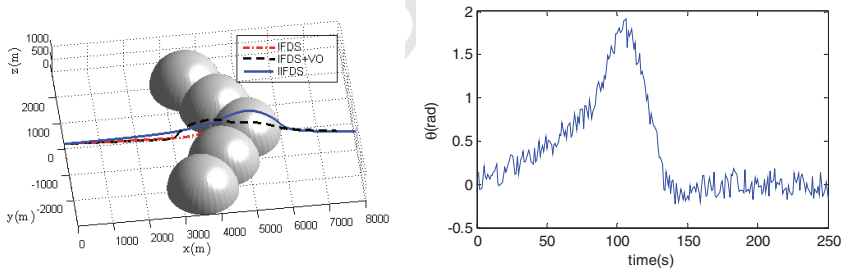

(a)Results by different methods (b) Tangential direction parameter *vs* time

Fig. 14 Process of avoiding trap area

6.3 Cooperative target tracking and obstacle avoidance

In this scenario, it is supposed that three UAVs need avoid moving threats or static obstacles when they are tracking a moving target. Hence the hybrid method by combing LGVF and IIFDS is adopted here. Suppose that there are two moving threats in planning space. One can be regarded a cone, whose motion information is: $x=8000-10t$, $y=800+300\sin(0.05t)$, and $z=0$. The other is a cylinder with the motion information: $x=4000-7t$, $y=-2000+9t+300\sin(0.05t)$, and $z=0$. Besides, there is a static sphere obstacle with radius 1000m. Based on the expansion parameters of obstacle, the safe distance between UAVs and threat surface is d_{buffer}=100m .

Fig. 15 displays the planned paths by LGVF+IIFDS. Fig. 16 illustrates the distance between each UAV and the cylinder obstacle surface i.e. $d_{\text{UAV1-threat1}}$, $d_{\text{UAV2-threat1}}$ and $d_{\text{UAV3-threat1}}$, and the distance between UAV and the cone obstacle surface i.e. $d_{\text{UAV1-threat2}}$, $d_{\text{UAV2-threat2}}$ and $d_{\text{UAV3-threat2}}$. It is obvious that all the distances are bigger than d_{buffer}, meaning that the three UAVs will avoid moving threats successfully. As we see, IIFDS method has good property of obstacle avoidance. Fig. 17 displays the spacing of UAVs i.e. $d_{\text{UAV1-UAV2}}$, $d_{\text{UAV1-UAV3}}$ and $d_{\text{UAV2-UAV3}}$, all of which are bigger than d_{safe} and smaller than d_{inf}, so the

spacing constraints of collaborative mechanism are satisfied. Besides, the horizontal distance between UAV and target, the UAV height are displayed in Fig.18 and Fig.19 respectively. It is inevitable that UAVs will deviate from the limit cycle as the obstacle avoidance behavior occurs. But UAVs will be back to the limit cycle once they have avoided the obstacle safely. Therefore, the tasks of target tracking and obstacle avoidance are well performed simultaneously.

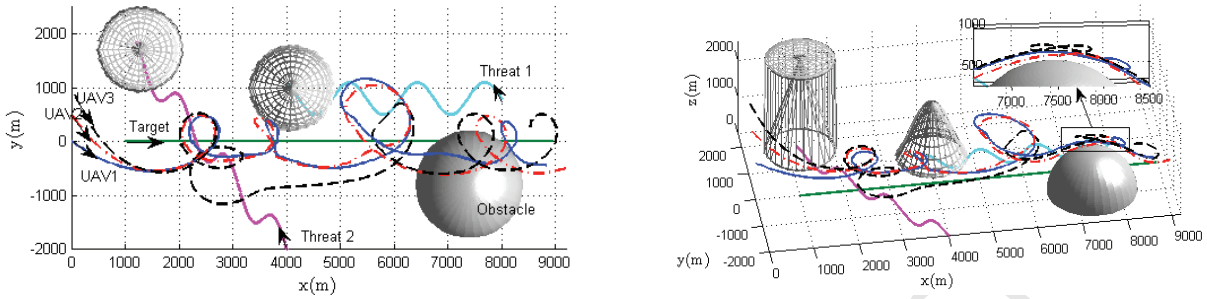

(a) 2D paths in x-y plane (b) 3D paths

Fig. 15 Collaborative path planning

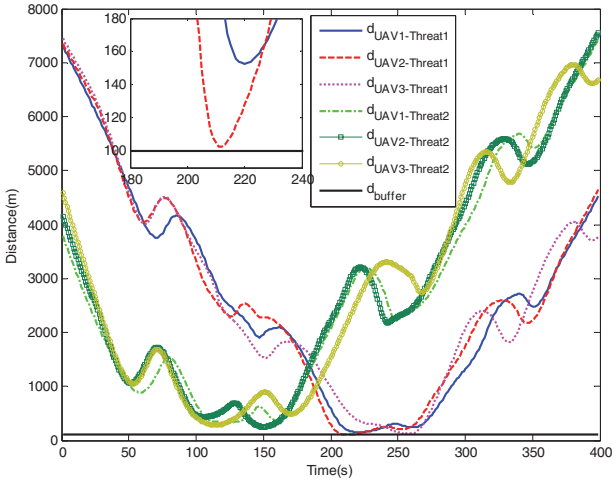

Fig. 16 Distance between UAVs and threats

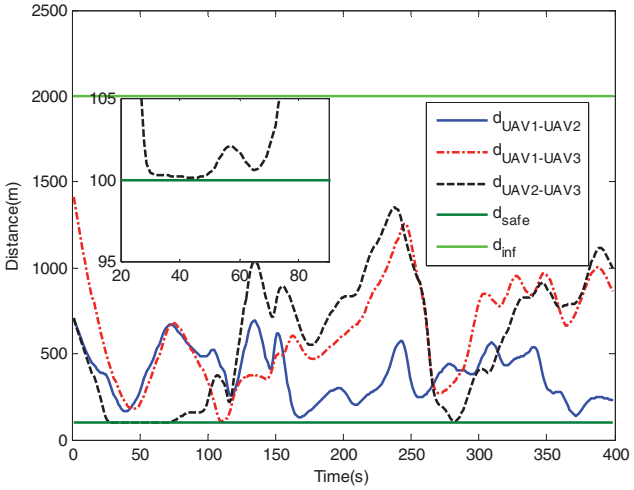

Fig. 17 Spacing of UAVs

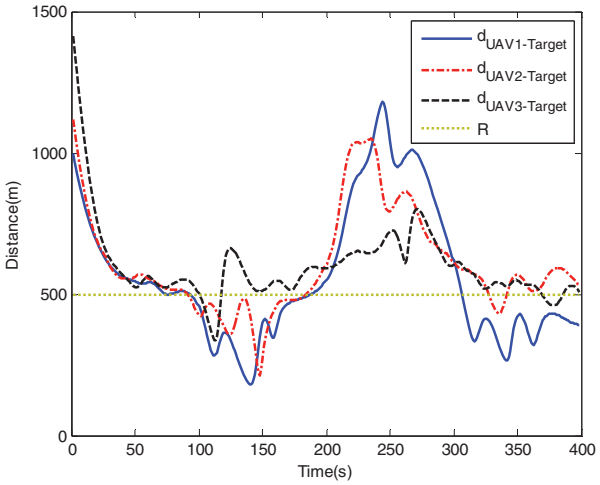

Fig. 18 Horizontal distance between UAV and target

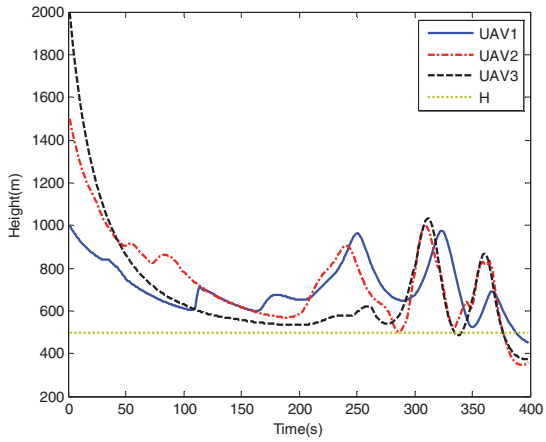

Fig. 19 Height of UAVs

6.4 Strategy of rolling optimization

A complicated dynamic scenario is constructed here. Some static obstacles are generated randomly in the planning space, and one cylinder threat with radius 500m moves as follows: $x = 2100 + 15t$, $y = 2300 - 15t + 200\sin(0.1t)$ and $z = 0$. Hence the safe distance between UAV and threat surface is d_{buffer}=60m. The target moves in the x-y plane with the motion model: $x = 5000\cos(0.004t)$, $y = 5000\sin(0.004 \cdot t)$ and $z = 0$, $t \in [0, 400]$. Three UAVs will perform the tasks with the initial positions $(0, 0, 1200)$ m, $(0, 250, 1000)$ m, and $(0, 500, 800)$ m.

Fig. 20 shows the paths by LGVF+IIFDS method with the one-step planning strategy. The one-step strategy actually means that the rolling optimization strategy is not performed. By the one-step strategy, only the current information of target or threat is considered and hence only the UAV behavior of next time is planned. As shown in Fig. 20, although the paths can avoid obstacles and track targets, the path quality especially the smoothness is poor. As shown in Fig. 21, if the rolling adjustment strategy is adopted (N=5), the routes will be much smoother as the future motion is considered beforehand.

With different horizon lengths (N=1, 3, 5, 7), the evaluations of the corresponding path of UAV2 are shown quantitatively in Table 3. All the paths can avoid the moving threat safely i.e. $\min d_{\text{UAV-threat}} \geq d_{\text{buffer}}$ always holds. The definition of global smoothness GS and local smoothness LS can be seen in Ref [20]. If the one-step strategy is utilized, the global smoothness GS, the turn rate $\dot{\psi}$, the flight path angle γ and the air speed v are out of their respective ranges at times, so the path is unfeasible. If N is too large (N=7), the planning time T_{p} may be larger than the sampling time ΔT, meaning that the path cannot be planned in real time. With a reasonable horizon length (N=3 or 5), the time T_{p} will be less than ΔT, i.e. the paths can be planned online. What's more, the path with N=3 or 5 is feasible, the quality of which is much higher than that by one-step strategy. Further, by comparing the performances with N=3 and N=5, the path quality of the latter is better.

Table.3. Performances of paths with different N

Performance	N=1	N=3	N=5	N=7
Range of T_p (s)	[0.01,0.12]	[0.20,0.48]	[0.67,0.89]	[0.97,1.34]
min $d_{\text{UAV-threat}}$ (m)	65	72	70	67
GS(deg)	106.7	28.6	24.8	24.5
LS(deg)	5.87	5.44	4.88	4.76
γ (deg)	[-55.8,52.6]	[-21.0,19.1]	[-18.8,17.2]	[-15.8,16.5]
$\dot{\psi}$ (deg/s)	[-79.3,80.2]	[-26.3,24.8]	[-20.6,19.3]	[-16.6,17.5]
v (m/s)	[15.2,310.0]	[31.1,65.9]	[33.2,69.5]	[30.2,68.9]

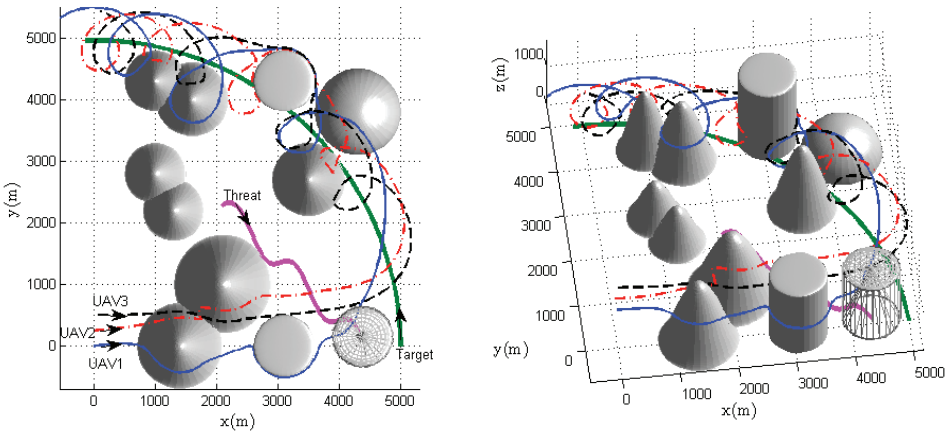

(a)2D paths in x-y plane (b) 3D paths

Fig. 20 One-step strategy

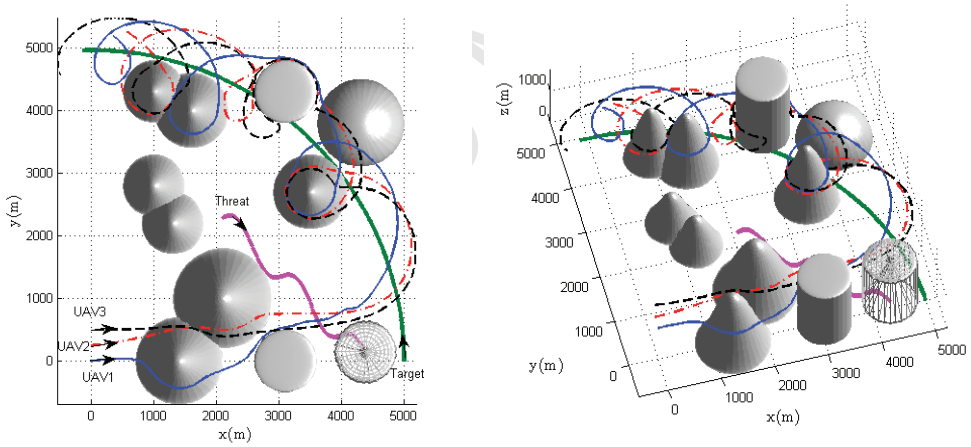

(a)2D paths in x-y plane (b) 3D paths

Fig. 21 Rolling optimization strategy (N=5)

7. Conclusion

This paper focuses on solving the problem of cooperative path planning with applications to target tracking and obstacle avoidance in 3D complex environment. LGVF is utilized for stand-off target tracking in 3D environment. Then IIFDS method is proposed for obstacle avoidance and the local minimum problem is eliminated. For collaborative mechanism, the strategies of virtual obstacle and extra-attraction fluid are added into IIFDS framework. Then LGVF and IIFDS are combined skillfully to simultaneously achieve the requirements of two missions, and the reactive parameters are optimized in the rolling horizon. This hybrid strategy combines the advantages of LGVF and IIFDS. Compared to other methods, it has the superiorities e.g. higher route quality, less calculation time and stronger practicality. In our future research, we will implement the method on a real UAV platform.

Conflict of interest statement

The authors declare that they do not have any conflicts of interest to this work.

Acknowledgement

The authors would like to express their acknowledgement for the support from the National Natural Science Foundation of China (No. 61175084), Program for Changjiang Scholars and Innovative Research Team in University (No. IRT13004).

References

[1] X. Zhang, J. Chen, B. Xin, et al., A memetic algorithm for path planning of curvature-constrained UAVs performing surveillance of multiple ground targets, Chin. J. Aeronaut. 27(3) (2014) 622-633.

[2] W.R. Zhu, H.B. Duan, Chaotic predator-prey biogeography-based optimization approach for UCAV path planning, Aerosp. Sci. Technol. 32 (2014) 153-161.

[3] F. Ahmed, K. Deb, Multi-objective optimal path planning using elitist non-dominated sorting genetic algorithms, Soft Comput. 17(7) (2013) 1283-1299.

[4] V. Shaferman, T. Shima, Tracking multiple ground targets in urban environments using cooperating unmanned aerial vehicles, J. Dyn. Syst-T. Asme 137(5) (2015) 1-11.

[5] H. Oh, S. Kim, H.S. Shin, et al., Rendezvous and standoff target tracking guidance using differential geometry, J. Intell. Robot Syst. 69 (2013) 389-405.

[6] S. Kim, H. Oh, A. Tsourdos, Nonlinear model predictive coordinated standoff tracking of a moving ground vehicle, J. Guid. Control Dynam. 36(2) (2013) 557-566.

[7] S.A.P. Quintero, F. Papi, D.J. Klein, et al., Optimal UAV coordination for target tracking using dynamic programming, in: 49th IEEE Conference on Decision and Control, Dec. 2010, IEEE Paper 4541-4546.

[8] E.W. Frew, D.A. Lawrence, S. Morris, Coordinated standoff tracking of moving targets using Lyapunov guidance vector fields, J. Guid. Control Dynam. 31(2) (2008) 290-306.

[9] H.D. Chen, K.C. Chang, C.S. Agate, A dynamic path planning algorithm for UAV tracking, in: Proceedings of the International Society for Optical Engineering, 2009, SPIE Paper 7336:B1-10.

[10] H.D. Chen, K.C. Chang, C.S. Agate, UAV path planning with Tangent-plus-Lyapunov vector field guidance and obstacle avoidance, IEEE T. Aero. Elec. Sys. 49(2) (2013) 840-856.

[11] R. Wise, R. Rysdyk, UAV coordination for autonomous target tracking, in: AIAA Guidance, Navigation, and Control Conference and Exhibit, Aug. 2006, AIAA paper: 2006-6453.

[12] J. Narkiewicz, A. Kopyt, T. Małecki, P. Radziszewski, Optimal selection of UAV for ground target tracking, in: AIAA Aviation, Jun. 2015, AIAA paper: 2015-2330.

[13] S. Ragi, E.K.P. Chong, UAV path planning in a dynamic environment via partially observable Markov decision process, IEEE T. Aero. Elec. Sys. 49(4) (2013) 2397-2412.

[14] J-W Lee, B. Walker, K. Cohen, Path planning of unmanned aerial vehicles in a dynamic environment, in: Infotech@Aerospace 2011, Mar. 2011, AIAA paper: 2011-1654.

[15] J. Wilburm, M.G. Perhinschi, B. Wilburn, O. Karas, Development of a modified Voronoi algorithm for UAV path planning and obstacle avoidance, in: AIAA Guidance, Navigation, and Control Conference, Aug. 2012, AIAA paper: 2012-4904.

[16] J. Holub1, J.L. Foo, V. Kilivarapu, E. Winer, Three dimensional multi-objective UAV path planning using digital pheromone particle swarm optimization, in: 53rd AIAA/ASME/ASCE/AHS/ASC Structures, Structural Dynamics and Materials Conference, Apr. 2012, AIAA paper: 2012-1525.

[17] V. Roberge, M. Tarbouchi, G. Labonte, Comparison of parallel genetic algorithm and particle swarm optimization for real-time UAV path planning, IEEE T. Ind. Inform. 9(1) (2013) 132-141.

[18] D. Levine, B. Luders, J. P. How, Information-rich path planning with general constraints using rapidly-exploring random trees, in: AIAA Infotech@Aerospace 2010, Apr. 2010, AIAA paper: 2010-3360.

[19] J. Ruchti, R. Senkbeil, J. Carroll, et al., Unmanned aerial system collision avoidance using artificial potential fields, Journal of Aerospace Information Systems, 11(3) 2014 140-144.

[20] Z. Zheng, S.J. Wu, W. Liu, et al., A feedback based CRI approach to fuzzy reasoning, Appl. Soft comput. 11(1) (2011) 1241-1255.

[21] B.C. Zhang, W.Q. Liu, Z.L. Mao, et al., Cooperative and geometric learning algorithm (CGLA) for path planning of UAVs with limited information, Automatica 50(3) (2014) 809-820.

[22] D. Bauso, L. Giarre, R. Pesent, Multiple UAV cooperative path planning via neuro-dynamic programming, in: 2004 43th IEEE conference on decision and control, Dec. 2004, IEEE paper 1087-1092.

[23] P. Yao, H.L. Wang, C. Liu, 3-D dynamic path planning for UAV based on interfered fluid flow, in: 2014 IEEE Chinese Guidance, Navigation and Control Conference, Aug. 2014, IEEE Paper 997-1002.

[24] H.L. Wang, W.T. Lyu, P. Yao, et al., Three-dimensional path planning for unmanned aerial vehicle based on interfered fluid dynamical system, Chin. J. Aeronaut. 28(1) (2015) 229-239.

[25] P. Yao, H.L. Wang, Z.K. Su, Real-time path planning of unmanned aerial vehicle for target tracking and obstacle avoidance in complex dynamic environment, Aerosp. Sci. Technol. 47 (2015) 269-279.

[26] P. Yao, H.L. Wang, Z.K Su, UAV feasible path planning based on disturbed fluid and trajectory propagation, Chin. J. Aeronaut. 28(4) (2015) 1163-1177.

[27] Y. Bar-Shalom, X.R. Li, T. Kirubarajan, Estimation with applications to tracking and navigation: Theory, Algorithm and Software, John Wiley and Sons Inc., New York, 2001.

[28] I. Karimi, S.H. Pourtakdoust, Optimal maneuver-based motion planning over terrain and threats using a dynamic hybrid PSO algorithm, Aerosp. Sci. Technol. 26(1) (2013) 60-71.